

Supplementary Information for

Multiscale Structured Low-Temperature Solid Oxide Fuel Cells with 13 W Power at 500 °C

Sung Soo Shin,^{abc} Jeong Hun Kim,^{cd} Kyung Taek Bae,^e Kang-Taek Lee,^f Sang Moon Kim,^g Ji-
Won Son,^{ch} Mansoo Choi^{*ab} and Hyoungchul Kim^{*c}

^a*Department of Mechanical and Aerospace Engineering, Seoul National University, 1 Gwanak-ro, Seoul 08826, Republic of Korea*

^b*Global Frontier Center for Multiscale Energy Systems, Seoul National University, 1 Gwanak-ro, Seoul 08826, Republic of Korea*

^c*Center for Energy Materials Research, Korea Institute of Science and Technology, 5 Hwarang-ro 14-gil, Seongbuk-gu, Seoul 02792, Republic of Korea*

^d*Emerging Materials Research Section, Electronics and Telecommunications Research Institute, 218 Gajeong-ro, Yuseong-gu, Daejeon 34129, Republic of Korea*

^e*Department of Energy Science and Engineering, Daegu Gyeongbuk Institute of Science and Technology, 333 Technojungang-daero, Daegu 42988, Republic of Korea*

^f*Department of Mechanical Engineering, Korea Advanced Institute of Science and Technology, 291 Daehak-ro, Yuseong-gu, Daejeon 34141, Republic of Korea*

^g*Department of Mechanical Engineering, Incheon National University, 119 Academy-ro, Yeonsu-gu, Incheon 22012, Republic of Korea*

^h*Graduate School of Energy and Environment (KU-KIST GREEN SCHOOL), Korea University, 145 Anam-ro, Seongbuk-gu, Seoul 02841, Republic of Korea*

*Corresponding author. E-mail address: mchoi@snu.ac.kr (M. Choi), hyoungchul@kist.re.kr (H. Kim)

Experimental

Fabrication of microscale patterned polymer molds. A silicon master with wet-etched square-pyramid pattern (a square base with all edges of length 6 μm , pattern spacing of 4 μm) was prepared to fabricate the polymer mold. To fabricate the poly-dimethylsiloxane (PDMS; Sylgard 184, Dow Corning) replica from the silicon master, the PDMS elastomer base and curing agent were mixed in a weight ratio of 10:1. The mixed solution was poured on the master and thermally cured for 1 h at 70 $^{\circ}\text{C}$. The cured PDMS replica was then carefully removed from the master mold and precisely cut for fabrication of the polyurethane acrylate (PUA; MINS 311RM, Minuta Tech.) mold. Subsequently, a small amount of PUA was dropped onto a PDMS replica, and a polyethylene terephthalate (PET) film with a thickness of 250 μm was lightly pressed against the dropped PUA resin. The assembly was then cured with ultra-violet (UV) light (Fusion Cure System, Minuta Tech.) for 5 min. After the removal of the PDMS replica, we performed final curing of the cured PUA mold with UV exposure for 12 h.

Additionally, a 6 cm \times 6 cm large-area pyramidally patterned PUA mold was prepared for large-area 3D architected (3DA) cell fabrication. We attached a black mask film with a 2 cm \times 2 cm small-area PDMS replica sized open window to the back of the PET film. Then, a small amount of PUA was added dropwise onto the PET film in the open window site and slightly press with the PDMS replica (negative structures). By inverting the assembly and curing with UV light, a pyramidally patterned PUA structure was produced on the PET film. The above procedure was repeated several times to fabricate a large-area multi-arrayed PUA mold (positive structures). Then, a large-area multi-arrayed PUA mold (negative structures) was fabricated by Teflon coating the multi-arrayed PUA mold and subsequent patterning process.

Fabrication of microscale patterned anode-support. Ceramic tape-casting and thermal lamination processes were used to fabricate an anode support for the 3DA-cells and Planar-cells. Slurries were prepared for the tape casting composed of 8 mol % Y_2O_3 -stabilized ZrO_2 (YSZ; Tosho) and NiO

(Sumitomo) powders in a weight ratio of 44:56 for the YSZ-based cells and $\text{Ce}_{0.9}\text{Gd}_{0.1}\text{O}_{1.95}$ (CGO; Rhodia) and NiO powders in a weight ratio of 49:51 for the CGO-based cells. Ethyl alcohol and toluene were used as base solvents, and dibutyl phthalate (Sigma Aldrich), KD-1 (Sigma Aldrich), and polyvinyl butyral (Sigma Aldrich) were utilized as the plasticizer, dispersant, and binder, respectively. Anode tape sheets were prepared for the anode substrate, which included the pore-forming additive, polymethyl methacrylate (Sunjin Chemical), and an anode-functional layer (AFL) without a pore former. For the one-step imprinting process, a multilayered anode substrate was fabricated with a thickness of 1 mm by stacking several sheets of NiO-YSZ or NiO-CGO tapes, a sheet of AFL, and the pyramidally patterned PUA mold at a pressure of 14.89 MPa at 80 °C for 15 min. The pyramidally patterned anode body was sintered at 1300 °C for 4 h. The sintered anode support was cut into 2 cm × 2 cm or 5 cm × 5 cm pieces for preparation of the full cell.

Fabrication of solid oxide fuel cells. The following deposition process was employed for cell fabrication, and was conducted using various thin-film deposition techniques. A radiofrequency (RF) sputtering system and a pulsed-laser deposition (PLD) process were employed for the respective deposition of electrolyte and cathode materials. A nanoscale anode-functional layer (nAFL) composed of NiO-YSZ or NiO-CGO was deposited over the sintered anode support with the use of magnetron RF sputtering (NiO:YSZ = 56:44 wt %; NiO:CGO = 51:49 wt %). To densify the nAFL and prevent Ni agglomeration, the anode support was annealed for 1 h at 1200 °C. Both YSZ and CGO layers were deposited over the densified nAFL using sputtering. In all of the sputtering process, an RF power of 100 W and a substrate temperature of 700 °C were applied, and the ambient argon gas was used at a pressure of 5 mTorr. The deposition times of nAFL, YSZ, and CGO layers for YSZ-based cells, were set at 12, 6, and 2 h, respectively. And the deposition time of nAFL, CGO, YSZ, and CGO layers for CGO-based cells, were set at 12, 6, 0.5, and 1 h, respectively. To fabricate a dense electrode with an area of 1 cm × 1

cm and 4 cm × 4 cm, LSC was deposited over the CGO layer using PLD for 2 h and 4 h at an ambient oxygen pressure of 300 mTorr and a substrate temperature of 700 °C.

Characterization of solid oxide fuel cells. The variations of the elastic modulus of the anode substrate were measured using a transverse rupture strength testing machine (5982, INSTRON) as a function of temperature (25 to 1300 °C). An anode substrate of width 5 mm, length 10 mm, and thickness 1 mm was prepared as a specimen for each temperature value of the thermal annealing profile including debinding and sintering steps. During the electrochemical performance test, air and 3 % humidified hydrogen were fed as the oxidant and the fuel. The open-circuit voltage (V_{OC}) and electrochemical performances of the cells were analyzed at three different temperatures, and electrochemical impedance spectroscopy (EIS) was conducted with an electrochemical analyzer (Iviumstat, Ivium Technologies) at a broad frequency range of 0.1 to 1×10^6 Hz. To observe the microstructures of the cells, we used a scanning electron microscopy (SEM; Regulus 8230, Hitachi), transmission electron microscopy (TEM; Talos F200X, FEI), and a focused-ion beam (FIB; Helios NanoLab 600, FEI) system. The 3D reconstruction processes of the 3DA-cells and Planar-cells were conducted using a FIB–SEM, dual beam system. To prepare the specimen for FIB tomography, epoxy resin (EpoVac System, Struers) was infiltrated onto the cathode and cured for one day. After overnight curing, repeated FIB slicing and SEM imaging were performed with a thickness of 30 nm along the z -axis. Subsequently, 3D reconstructions from both cells were analyzed based on additional processes (*e.g.*, aligning, sectioning, trimming, and characterizing), and the structural variables were measured with the Avizo 9.0 software package (FEI VSG).

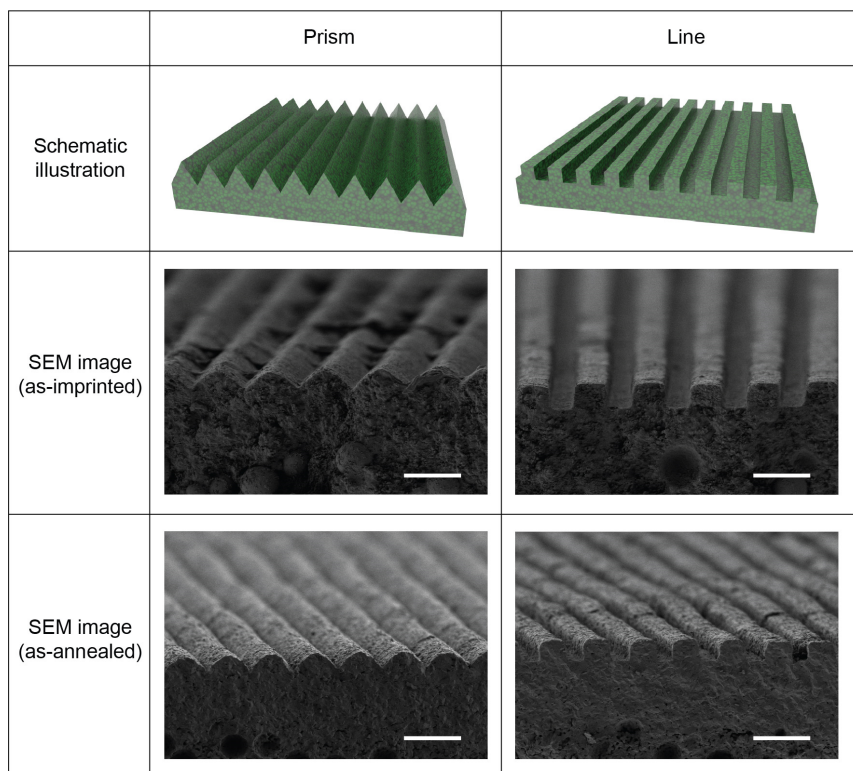


Fig. S1. Schematics and SEM images of as-imprinted and as-annealed states of prism- and line-shaped NiO–YSZ structures. All scale bars correspond to 10 μm .

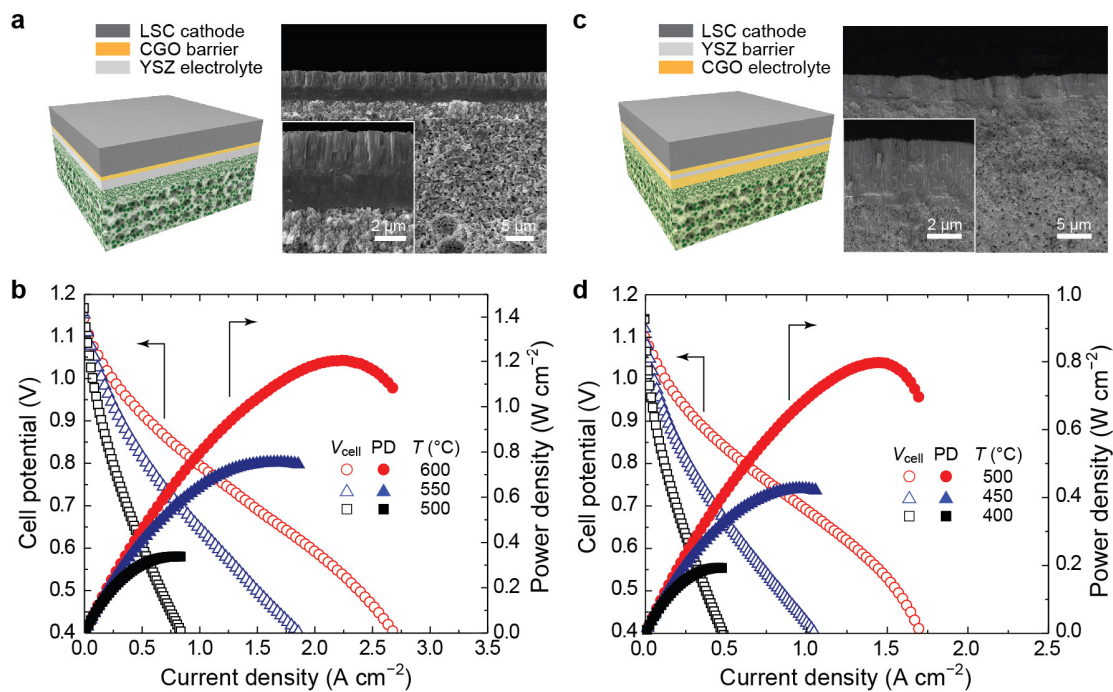


Fig. S2. (a) Schematic illustration (left) and SEM images (right) of an YSZ-based Planar-cell. The inset depicts the magnified SEM image of a planar structure. (b) Potential and power density curves of YSZ-based Planar-cells at three different temperatures. (c) Schematic illustration (left) and SEM images (right) of a CGO-based Planar-cell. The inset depicts the magnified SEM image of a planar structure. (d) Potential and power density curves of CGO-based Planar-cells at three different temperatures. All experiments were performed under a feeding of air and 3 % humidified hydrogen at a rate 200 mL min⁻¹.

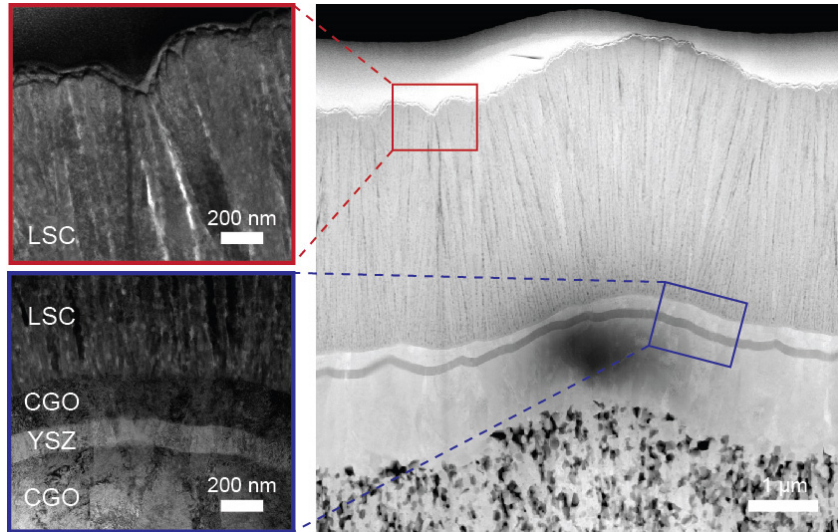


Fig. S3. Cross-sectional TEM images of a CGO-based 3DA-cell showing the pyramidal 3D architectures and interfacial microstructures. Close-up TEM images from the top of LSC (red region) and the interface of LSC and CGO/YSZ/CGO electrolyte (blue region).

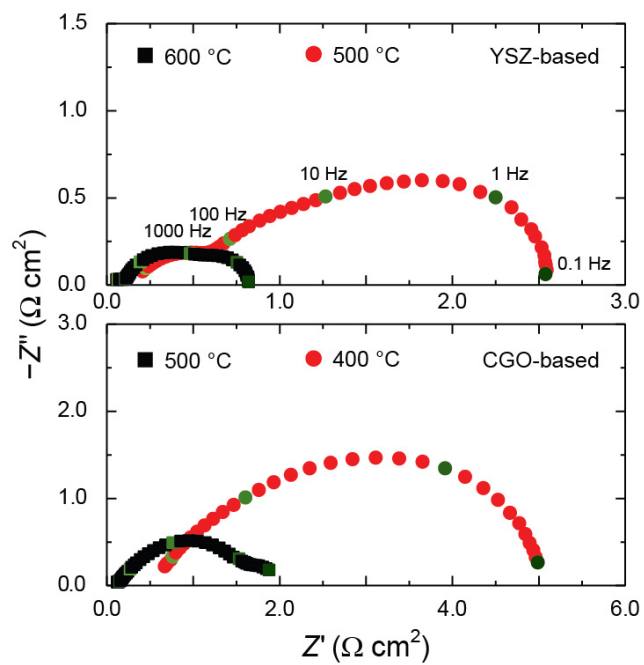


Fig. S4. EIS spectra of YSZ- and CGO-based 3DA-cells measured at V_{OC} condition.

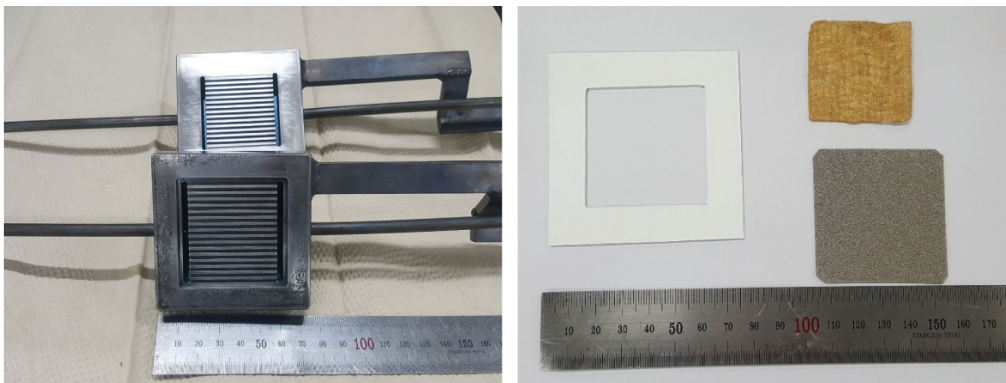


Fig. S5. Used jig(left), glass-ceramic sealant, Au mesh cathode current collector and Ni foam anode current collector(right) for large-area CGO-based 3DA-cell measurement.

Table S1. Comparison of electrochemical performance in this work with those of the previously reported ceramic fuel cells for low-temperature operation. The ‘*’ symbols indicate that the area of anode green body was used as the active area due to the lack of information in the articles. Also, the ‘**’ symbol indicates that the area of anode sintered body was used as the active area due to the lack of information in the article.

Type	Ref.	Active area (mm ²)	PD _{max} (W cm ⁻²)	P _{total} (W)	T (°C)	Degradation rate (Total operation time)
SOFC	1	115	1.22	1.38	500	0.09% per h (150h)
	2	79	1.58	1.24	500	0.02% per h (250 h)
	3	550	0.156	0.83	500	N/A
	4	48	1.02	0.49	500	N/A
	5	46	0.91	0.42	500	0.15% per h (164 h)
	6	20	0.97	0.19	500	Negligible (2500 h)
	7*	177	0.71	1.255	500	Negligible (150 h)
	8*	177	0.662	1.17	500	Negligible (150 h)
	9	48	0.561	0.269	500	N/A
	10	28	0.47	0.132	500	N/A
	11	20	0.74	0.145	500	N/A
	12*	255	0.589	1.499	500	N/A
	13	32	0.62	0.223	500	Negligible (260 h)
	14*	177	0.601	1.062	500	Negligible (100 h)
micro-SOFC	15	0.16	0.186	2.98×10 ⁻⁴	450	N/A
	16	0.36	0.864	3.1×10 ⁻³	450	N/A
	17	0.03	1.3	3.85×10 ⁻⁴	450	30% per h
	18	0.01	1.34	1.34×10 ⁻⁴	500	20% per h
	19	1.27	0.317	4.01×10 ⁻³	400	N/A
	20	13.5	0.155	0.021	510	14% per h
PCFC	21	1600	0.535	8.56	500	0.07% per h
	22*	284	0.405	1.148	500	Negligible (1100 h)
	23**	216	0.587	1.27	500	N/A
	24	100	0.35	0.35	500	N/A
	25	28	0.548	0.153	500	Negligible (700 h)
	26	64	0.643	0.412	500	Negligible (26 h)
SOFC	This work	1600	0.83	13.27	500	0.05% per 500 h

References

- 1 M. Li, M. Zhao, F. Li, W. Zhou, V. K. Peterson, X. Xu, Z. Shao, I. Gentle and Z. Zhu, *Nat. Commun.*, 2017, **8**, 13990.
- 2 J. G. Lee, J. H. Park and Y. G. Shul, *Nat. Commun.*, 2014, **5**, 4045.
- 3 H. Shi, G. Yang, Z. Liu, G. Zhang, R. Ran, Z. Shao, W. Zhou and W. Jin, *Int. J. Hydrogen Energy*, 2012, **37**, 13022–13029.
- 4 Y. Zhu, Z.-G. Chen, W. Zhou, S. Jiang, J. Zou and Z. Shao, *ChemSusChem*, 2013, **6**, 2249–2254.
- 5 W. Zhou, J. Sunarso, M. Zhao, F. Liang, T. Klande and A. Feldhoff, *Angew. Chem. Int. Ed.*, 2013, **52**, 14036–14040.
- 6 C. Duan, D. Hook, Y. Chen, J. Tong and R. O’Hayre, *Energy Environ. Sci.*, 2017, **10**, 176–182.
- 7 S. Choi, S. Yoo, J. Kim, S. Park, A. Jun, S. Sengodan, J. Kim, J. Shin, H. Y. Jeong, Y. Choi, G. Kim and M. Liu, *Sci. Rep.*, 2013, **3**, 2426.
- 8 S. Yoo, A. Jun, Y.-W. Ju, D. Odkhoo, J. Hyodo, H. Y. Jeong, N. Park, J. Shin, T. Ishihara and G. Kim, *Angew. Chem. Int. Ed.*, 2014, **53**, 13064–13067.
- 9 W. Zhou, Z. Shao, R. Ran, W. Jin and N. Xu, *Chem. Commun.*, 2008, **44**, 5791–5793.
- 10 D. Han, X. Liu, F. Zeng, J. Qian, T. Wu and Z. Zhan, *Sci. Rep.*, 2012, **2**, 462.
- 11 Y.-W. Ju, J. Hyodo, A. Inoishi, S. Ida and T. Ishihara, *J. Mater. Chem. A*, 2015, **3**, 3586–3593.
- 12 J. G. Lee, M. G. Park, S.-H. Hyun and Y. G. Shul, *Electrochim. Acta*, 2014, **129**, 100–106.
- 13 Y. Chen, Y. Bu, B. Zhao, Y. Zhang, D. Ding, R. Hu, T. Wei, B. Rainwater, Y. Ding, F. Chen, C. Yang, J. Liu and M. Liu, *Nano Energy*, 2016, **26**, 90–99.

- 14 J. Kim, S. Choi, A. Jun, H. Y. Jeong, J. Shin and G. Kim, *ChemSusChem*, 2014, **7**, 1669–1675.
- 15 Y. B. Kim, T. M. Gür, S. Kang, H.-J. Jung, R. Sinclair and F. B. Prinz, *Electrochem. commun.*, 2011, **13**, 403–406.
- 16 P.-C. Su, C.-C. Chao, J. H. Shim, R. Fasching and F. B. Prinz, *Nano Lett.*, 2008, **8**, 2289–2292.
- 17 J. An, Y.-B. Kim, J. Park, T. M. Gür and F. B. Prinz, *Nano Lett.*, 2013, **13**, 4551–4555.
- 18 C.-C. Chao, C.-M. Hsu, Y. Cui and F. B. Prinz, *ACS Nano*, 2011, **5**, 5692–5696.
- 19 J. D. Baek, C.-C. Yu and P.-C. Su, *Nano Lett.*, 2016, **16**, 2413–2417.
- 20 M. Tsuchiya, B.-K. Lai and S. Ramanathan, *Nat. Nanotechnol.*, 2011, **6**, 282–286.
- 21 H. An, H.-W. Lee, B.-K. Kim, J.-W. Son, K. J. Yoon, H. Kim, D. Shin, H.-I. Ji and J.-H. Lee, *Nat. Energy*, 2018, **3**, 870–875.
- 22 C. Duan, J. Tong, M. Shang, S. Nikodemski, M. Sanders, S. Ricote, A. Almansoori and R. O’Hayre, *Science*, 2015, **349**, 1321–1326.
- 23 S. H. Nien, C. S. Hsu, C. L. Chang and B. H. Hwang, *Fuel Cells*, 2011, **11**, 178–183.
- 24 S. M. Choi, H. An, K. J. Yoon, B.-K. Kim, H.-W. Lee, J.-W. Son, H. Kim, D. Shin, H.-I. Ji and J.-H. Lee, *Appl. Energy*, 2019, **233–234**, 29–36.
- 25 S. Choi, C. J. Kucharczyk, Y. Liang, X. Zhang, I. Takeuchi, H.-I. Ji and S. M. Haile, *Nat. Energy*, 2018, **3**, 202–210.
- 26 C. Xia, Y. Mi, B. Wang, B. Lin, G. Chen and B. Zhu, *Nat. Commun.*, 2019, **10**, 1707.